Wood Chemistry

Disan Gunbilig*, Notburga Gierlinger, Paraskevi Charalambous, Claudia Gusenbauer, Stefan Böhmdorfer, Antje Potthast and Thomas Rosenau

Chemical, microscopic, and mechanical properties of Mongolian *Haloxylon ammodendron* wood

https://doi.org/10.1515/hf-2024-0118
Received December 17, 2024; accepted March 26, 2025;
published online April 22, 2025

Abstract: *Haloxylon ammodendron* is a small psammophyte tree that grows under challenging environmental conditions in the Mongolian Gobi Desert. It plays a key role in sustaining the structure and function of the Gobi ecosystem, and it is a commodity with high ecological value on the regional scale. In this study, thin cross-sections of the wooden trunk were used to determine the type of tree ring boundaries and axial parenchyma characteristics by Raman imaging. The wood samples were analysed for their content, composition, and radial distribution of extractives, which provided insight into the ultrastructure of the wood trunk as well as the transport and storage of various metabolites. The ecologic success of the *H. ammodendron* is in part due to the deployment of lignin both as a protective component and key structural material. The tree species appear to have a potential as a precursor for various applications, such as the development of lignocellulosic sorbent materials, activated carbons, etc. due to the high lignin content, while the structure permits few utilizations, including composite pulps, particle boards and panels etc.

Dedicated to the Laboratory of Plant Chemistry, ICCT, Mongolian Academy of Sciences on its 50th anniversary.

***Corresponding author: Disan Gunbilig**, Department of Chemistry, Institute of Chemistry of Renewable Resources, University of Natural Resources and Life Sciences, Vienna (BOKU), Konrad Lorenz-Str. 24, 3430 Tulln, Austria, E-mail: gunbilig.disan@boku.ac.at
Notburga Gierlinger and Paraskevi Charalambous, Department of Bionanosciences, Institute for Biophysics, University of Natural Resources and Life Sciences, Vienna (BOKU), Muthgasse 11, 1190 Vienna, Austria
Claudia Gusenbauer, Department of Material Sciences and Process Engineering, Institute of Wood Technology and Renewable Materials, University of Natural Resources and Life Sciences, Vienna (BOKU), Konrad Lorenz-Str. 24, 3430 Tulln, Austria
Stefan Böhmdorfer, Antje Potthast and Thomas Rosenau, Department of Chemistry, Institute of Chemistry of Renewable Resources, University of Natural Resources and Life Sciences, Vienna (BOKU), Konrad Lorenz-Str. 24, 3430 Tulln, Austria. https://orcid.org/0000-0003-1981-2271 (A. Potthast). https://orcid.org/0000-0002-6636-9260 (T. Rosenau)

Keywords: chemical profile; lignin; mechanical properties; methanolysis; Raman imaging; *Haloxylon ammodendron*

1 Introduction

Haloxylon ammodendron, Chenopodiaceae (recently merged with Amaranthaceae) is a small psammophyte tree that is widely distributed in the arid regions of the Mongolian Plateau, particularly in the South and Southwest of the Gobi Deserts. It endures drought, high salinity, extreme temperatures, and intense solar radiation. While the entire forest of Mongolia has a total area of 11.7 million hectares, 3.8 million belong to the *H. ammodendron* forest. It is a commodity with ecological and economic values of ca. 27 million USD (Dorjsuren 2021) which is guarded by various regulatory mechanisms and governmental initiatives for afforestation, protection, and economic valorisation.

The tree species plays a key role in sustaining the structure and function of the Gobi ecosystem, where various desert communities (Liu et al. 2022) depend on the ecological success of *H. ammodendron*, as it forms nutrient-rich and low alkalinity/salinity fertile islands valuable for the desert ecosystem (Li et al. 2011). *H. ammodendron* is widely cultivated in many countries to prevent desertification and wind erosion, especially for anchoring sand dunes due to its massive roots and resilience to hot and dry conditions. However, *H. ammodendron* growing in Mongolia is largely underutilized, except for the fact that local residents exploit firewood from the naturally growing scrub forest. Another use is for artistic craft projects and souvenir production due to the waived grain pattern and texture of the wood, as well as naturally contorted shapes similar to ornamental bonsai trees. Other related species, i.e., *Haloxylon recurvum* and *Haloxylon salicornicum* have been used as firewood, fodder, and traditional medicines to cure both human and veterinary ailments, mostly intestinal ulcers, kidney pain, ear infections, insect stings, skin problems, etc. (Azhar et al. 2015).

Severe droughts, which occur on an interannual to decennial scale, and overgrazing due to the increase of livestock and wild ungulates affected the tree population and have

led to the degradation of a total of ca. 6,500 ha of *Haloxylon* forest in Mongolia only over the last decade. Projected scenarios through 2,100 (Hessl et al. 2018) are predicting above-average rates of temperature increase in the region (Liancourt et al. 2013), which will increasingly affect the plant community. Illegal collection of high-value materia medica, such as *Cynemorium songaricum*, and *Cistanche deserticola*, both holophrastic plants attached to the root of *H. ammodendron* considered an anthropogenic cause for the decline.

As sessile organisms, desert plants deploy various specialized and multifunctional metabolites and are fortified by the constitutive defense against environmental conditions and opponents, such as diseases and herbivores (Schneider 2022), at the trade-off of direct and indirect use of resources (Neilson et al. 2013). Fan et al. reported an upregulation of multiple genes for pathways associated with salt, osmotic, temperature, UV-, and high-intensity light stresses together with genes responsive to drought, suggesting an altered regulatory stress response system in *H. ammodendron* under water-deficient stress scenarios. In addition, *H. ammodendron* exhibited enhanced tolerance to biotic stress by down-regulating genes that were triggered in response to infection, showing a coordinated expression of genes that regulate stress tolerance and resource allocation to support survival of multiple stresses in the harsh desert environment (Fan et al. 2018).

The exploration of the chemical diversity of *H. ammodendron*, was aimed towards a better understanding of the adaptive plasticity of the plant, i.e., how it reacts against environmental stressors by *de novo* synthesis, transportation, and storage of specialized metabolites and plant polymers. One of them, lignin, is an extremely multi-faceted phenolic polymer, which is not only part of first-line plant defense (Lee et al. 2019; Menden et al. 2007; Moura et al. 2010; Tronchet et al. 2010) but also a key material for the cell ultrastructure of woody plants.

Therefore, the lignin, carbohydrate, and extractive profiles of Mongolian *H. ammodendron* species were studied with the help of various analytical techniques such as GC-MS and methanolysis (followed by GC–FID) for free sugar and hemicellulose content and composition. Additionally, Raman imaging was used to get insights into the anatomical structure and the distribution of the chemicals within the cell walls and across the tissue structure (Gierlinger 2017). Finally, the chemical and structural investigation was complemented with mechanical performance testing.

2 Materials and methods

2.1 Sampling

Wood samples of *H. ammodendron* were collected in the Bayanzag, South Gobi Province in Mongolia (coordinates: 44.1371, 103.7086) in July 2022. Solid pieces (approximately 10 × 30 cm) free from damages, stains, insect holes, etc. were sectioned from a living tree along the radial plane using a fine saw. They were stored under ambient conditions, in a cool and dark storage place until further analysis. A voucher specimen of the wood material was deposited at the MPG-MAS Joint Laboratory for Chemical Ecology in Ulaanbaatar, Mongolia.

2.2 *In situ* Raman imaging

Small wood blocks (approximately 5.0 × 5.0 mm) prepared from cross-sections by cutting along the grain direction were soaked for 24 h in D_2O, and air bubbles were removed using a vacuum pump. For cutting, the blocks were mounted on the sample holder by freezing with water (chamber temperature –13.0 °C), considering the cutting area and orientation (anatomical direction) of the wood beforehand. Cross sections (14.0 µm thickness) were cut from sapwood and heartwood using disposable microtome blades, (N35° Feather, Osaka Japan) and a cryo-microtome (CM3050 S, Leica Biosystems Nussloch GmbH, Wetzlar, Germany).

The sections were stained using a Fuchsin-Chrysoidine-Astrablue (FCA) solution (0.1 mg/mL of new Fuchsin, 0.143 mg/mL Chrysoidine, 1.25 mg/mL Astra blue and acetic acid (1:50, v/v)), followed by washing steps with distilled water, ethanol (30 %, 70 %) and *iso*-propanol. Microscopic pictures were taken on a light microscope (Labophot 2, Nikon, Tokyo, Japan). For Raman imaging, sections were placed together with a drop of water on a standard microscopy glass slide and sealed with a coverslip and nail polish (Mateu et al. 2020). Raman spectra were acquired using a confocal Raman microscope (alpha300RA, WITec, Wetzlar, Germany) equipped with a 100× oil immersion objective (NA 1.4, Carl Zeiss, Jena, Germany) as described earlier (Bock and Gierlinger 2019, Bock et al. 2019). A red diode laser (λ = 785 nm, WITec, Ulm, Germany) with a laser power of 200 mW was used for the experiments. The scattering signal was passed through an optic multifiber (100 µm) and was detected by a CCD camera (DU401A BR-DD, Andor, Belfast, North Ireland) behind the spectrometer (600 g/mm^{-1}, BLZ 750 nm, UHTS 300, WITec, Ulm, Germany). Several regions of interest were selected and mapped including sapwood and heartwood as well as different cell types. At every pixel one spectrum (80 cm^{-1} – 1,800 cm^{-1}) was acquired in 333 nm steps with an integration time of 0.04 s. Analysis of the data was performed with Project SIX Plus (WITec, Ulm, Germany) and Opus 7.5 software (Bruker Optik GmbH, Ettlingen, Germany). After removing cosmic ray interferences and correcting the baseline, Raman chemical images and average spectra were derived based on true component analysis (Morel and Gierlinger 2023).

2.3 Testing of mechanical properties

A compression test parallel to the grain was performed using a universal testing machine (Z100 Zwick-Roell, Ulm, Germany) according to the standard DIN52185. Cubic samples of 20.0 mm × 20.0 mm × 20.0 mm ± 1.0 mm were prepared from unsorted *H. ammodendron* disks using a circular saw. Before testing, the samples were conditioned (20.0 °C ± 2.0 °C and 65.0 % ± 5.0 % rel. humidity) according to ISO554 (International Organization for Standardization 1976) and the density was measured and calculated according to the standard DIN 52182 (Deutsches Institut für Normung 1976).

2.4 Isolation of extractives

The sample size was reduced using a cutting mill (Retsch SM1, Haan, Germany) equipped with sieves with an aperture size of 2.0 mm before the isolation of extractives and lignins. A total of 10.0 g of finely ground and sieved wood samples were subjected to accelerated solvent extraction (ASE 300, Dionex, Sunnyvale, USA). A sequential extraction scheme using 34.0 mL stainless steel cells, and solvents of different polarities, *i.e.*, n-hexane, acetone, and 70.0 % aqueous methanol, was performed under the following conditions: pressure 1,600.0 psi, temperature 50.0 °C, 5 min heat-up, 25 min static extraction with two cycles, and purging for 120 s using pressurized nitrogen gas. Extracts were collected and concentrated to dryness *in vacuo* until further research (not shown here). Wood samples were air-dried at room temperature to record the dry weight and for further isolation of both acid-insoluble and soluble lignins.

2.5 Isolation of lignins

Acid-insoluble lignin (or Klason lignin) was determined following the standard gravimetric assay described earlier (Lin and Dence 1992). Extractive-free samples were digested using an aqueous 72 wt% sulfuric acid. After filtration, the residue was washed with water and dried to mass constancy. The content of the lignin fraction soluble in 72 wt% sulfuric acid was determined in the hydrolysate (after the removal of the Klason lignin) by UV–vis spectroscopy at a wavelength of 205 nm (Lin and Dence 1992) after dilution with blank (1:1, v/v) such that its absorbance is in the range of 0.2–0.7 AU.

2.6 Acidic methanolysis

The carbohydrate composition in *H. ammodendron* wood samples was determined according to an acidic methanolysis protocol (Sundberg et al. 1996) after freeze drying. About 10.0 mg of the sample was weighed and soaked in 2.0 mL of 2 M HCl/MeOH. After thorough mixing (vortex) and ultrasonication, each for 2 min, the sample was heated for 5 h at 100.0 °C and cooled down to ambient temperature. The sample was mixed with the internal standard (sorbitol solution, 0.1 mg of sorbitol/mL methanol, 1.0 mL) before evaporation of the solvents under an N_2 stream, and lyophilization overnight. For GC analysis, 4-dimethylaminopyridine (DMAP/pyridine 1.5 mg/mL) and N,O-bis(trimethylsilyl)trifluoroacetamide (BSTFA with 10 % trimethylsilyl chloride) were added to the samples for derivatization at 70.0 °C for 2 h in accordance with (Becker et al. 2013a,b).

Ethyl acetate was added prior to analysis with GC–FID (Agilent Technologies model 7890B). GC parameters: sample injection volume, 1.0 mL; split ratio, 10:1. A HP1 (Agilent 19091Z413) methyl siloxane column (30.0 m × 320.0 mm × 0.25 mm) and He as a carrier gas at a flow rate of 2.0 mL/min were used for analysis. The oven temperature was programmed at 140.0 °C for 1 min, heated to 210.0 °C at 4.0 °C/min^{-1}, and then heated to 260.0 °C at 30.0 °C min^{-1} with a hold time of 5 min. The temperatures of the injector and detector were maintained at 260.0 °C and 280.0 °C, respectively. The FID temperature was fixed at 320.0 °C at a He flow rate of 30.0 mL min^{-1}.

2.7 Reagents

Solvents and internal standards were obtained from commercial suppliers: n-hexane, acetone, methanol, HCl, pyridine (Acros Organics, Geel, Belgium); sorbitol, 4-dimethylaminopyridine *N,O*-bis(trimethylsilyl)trifluoroacetamide (Sigma-Aldrich, St. Louis, USA); 2′-*O*-methyluridine-5′-triphosphate, 3′-*O*-methyluridine-5′-triphosphate, 5-methyluridine-5′-triphosphate (TriLink BioTechnologies, San Diego, USA).

3 Results and discussion

3.1 Microscopy and Raman imaging

Fuchsin-chrysoidin-astra blue (FCA) staining of the cross sections showed the distinct anatomical regions of the wood sample and provided an overview of the lignification sites. The red color indicates lignin in cell walls, while non-lignified cell walls appear blue (Figure 1).

In sapwood, the outer living water-conducting part of the tree, parenchyma cells surrounding the vessels stained blue as well as the cambial and phloem cells attached to the xylem (Figure 1A). Successive cambia are typical for Chenopodiaceae (Heklau et al. 2012) and offer an ecological advantage under water-deficiency stress conditions in

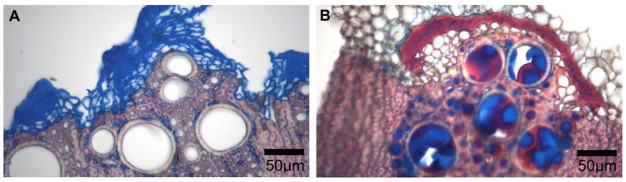

Figure 1: Microsection of *Haloxylon ammodendron* wood samples stained with FCA. (A) Sapwood stained distinguish lignified cell walls in vessels, tracheids, and fibers (stained in red) from unlignified parenchymatic cells (stained in blue). (B) In heartwood also thin-walled parenchyma and the sclerenchymatic fiber cup-stained red. Extractives stored in vessels and tracheids were stained either blue or red.

Haloxylon species (Nooshin 2012; Robert et al. 2011) as the radial increments sustain storage of water in the stem (Li et al. 2015). The vessels (60.0–70.0 µm) as well as the fibers were stained in light red due to lignified cell walls. In the *H. ammodendron* heartwood (Figure 1B) red staining was even more prominent, particularly in the very thick-walled fiber cells, tracheids, and the vessels. The latter ones were often filled with red as well as blue stained components, pointing to a high amount of diverse plant extractives, lining and filling the water-conducting elements of the heartwood. This was the first indicator that the desert wood structure was heavily impregnated with defense compounds to protect the plant organism against biotic and abiotic attacks (Kirker et al. 2013).

To reveal more details of the cell wall composition and the distribution of components in sapwood (Figure 2) and heartwood (Figure 3), the Raman imaging (Gierlinger 2017) technique was applied.

After stitching the whole microsection, different regions of interest were selected including fibers as well as vessels (Figure 2A). Within the acquired hyperspectral dataset, five very different spectral contributors (Figure 2B) were found, which were related to different cell types and cell wall layers (Figure 2C and D) and components between and within cells (Figure 2E–G). The S_2-layer of the cell wall of the thick-walled fibers (Figure 2C) was distinguished from the S_1-layer and the tracheid and vessel walls (Figure 2D). The corresponding spectra show the main difference to be in 1,122 cm^{-1}/1,095 cm^{-1} ratio, with a higher 1,095 cm^{-1} band and a lower 378 cm^{-1} band in the vessel and S_1-wall (in laser polarisation direction), see Figure 2B, blue (1) and cyan (2) spectra), higher cellulose microfibril angle in S_1 (Gierlinger et al. 2010). This result goes in line with the adaptation of fiber to tensile strength, characterized by a low cellulose microfibril angle, while the tracheid and vessel walls with their higher microfibril angle are specialized for compression strength parallel to grain to avoid buckling of the larger elements for water conduction.

Additionally, the higher lignin content in the vessel and tracheids means better hydrophobization and tightening of the wall for water transport. The highest lignification (Figure 2B, red spectrum 3 with pronounced 1,600.0 cm^{-1} band) is observed between the fibers (Figure 2E) in the cell zwickels and compound middle lamella, a unified pectin network important in fracture propagation between cell walls.

Two additional components were distinguished as lumen deposits (Figure 2F and G): one with high-background and noisy spectra due to fluorescence, probably due to aromatics (Figure 2B, orange spectrum 4), and another one with a band at 1,445.0 cm^{-1} pointing to lipids (Figure 2B, yellow spectrum 5). While the fluorescent aromatic component is attributed to the lumen of the fibers as well as the cell wall of the tracheids, the lipids are mainly found along ray cells as visualized in the combination image (Figure 2H). While the aromatics also seem to be extraneous to the cell wall and can thus influence natural durability and physico-mechanical properties, the lipids are storage components important to cope with changing environmental conditions and protect against pathogens or predators (N'Guessan et al. 2023).

In the heartwood, a region of interest was scanned (Figure 3A) in a similar way. Five different components were distinguished also here, spectra see Figure 3B. The first four spectra (Figure 3B, blue, cyan, red, orange) of the heartwood tissue and cell wall structures (Figure 3C–E) were similar to the corresponding sapwood counterparts (Figure 2B). The spectra were noisier due to the higher background (Figure 3B), since the fluorescing component (Figure 3F, extractives) is more heavily distributed throughout the whole tissue in heartwood than in sapwood (Figure 3F) and seems to contribute to the other component's spectra at every position. Unfortunately, no clear spectral signature was derived for this extractive component, which hinders further specification. A mixture of several (aromatic) extractive components is present in *Haloxylon*, which agrees with the spectroscopic observations in this study. The Raman scans revealed more impregnation of the tracheid and vessel area and a far-reaching fill-up of nearly all cell lumen (even in the fiber tissue) and confirmed a higher content of this component in heartwood than in sapwood (*cf.* Figure 2H–H). In heartwood, no lipids have been detected, but instead, crystals of calcium oxalate monohydrate (whewellite) (Figure 3G), identified based on the Raman doublet at 1,494.0 cm^{-1} and 1,465.0 cm^{-1}, together with the bands at 896.0 cm^{-1} can 503.0 cm^{-1} (Figure 3B, spectrum in black).

The $Ca(COO)_2$ monohydrate crystals were especially prominent at the border of vessels and fibers to the thin-walled cells (Figure 4A). The thick-walled fiber spectra (Figure 4B, blue spectrum 1) are different from the thin-walled cell wall spectra (Figure 4B, orange spectrum 2). From

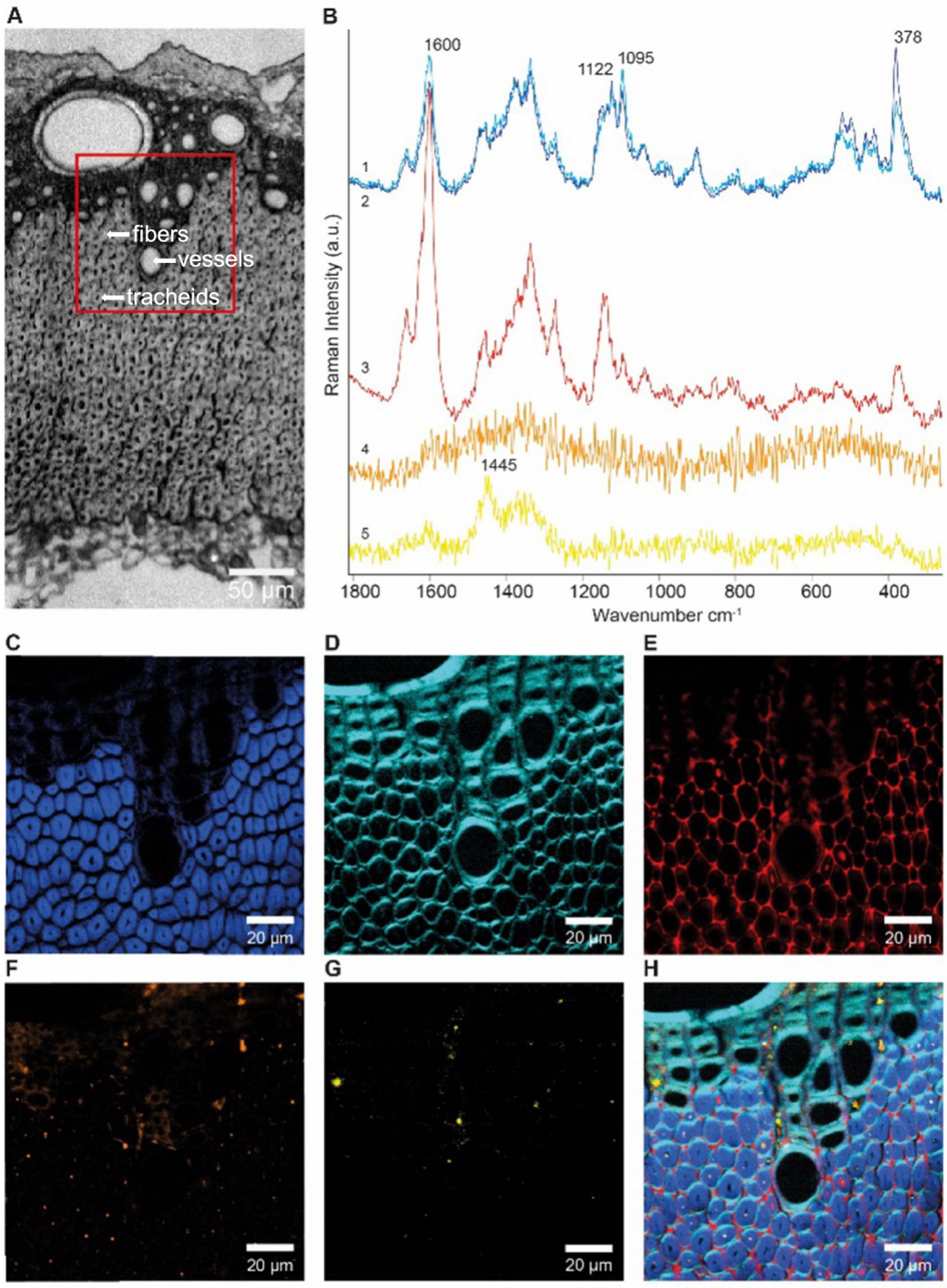

Figure 2: Raman images and spectra of *Haloxylon* sapwood derived by true component analysis. (A) Light microscopic stitching image showing the scanned region of interest including fibers as well as tracheids and vessels. (B) Five different component average spectra corresponding to (C–G). (C) Fibers building the main tissue with their cellulose-rich S_2 layers (blue spectrum). (D) S_1-layers of the fibers, tracheids, and vessels (cyan spectrum). (E) High-lignin regions in the middle lamella and cell zwickels (red spectrum, pronounced aromatic lignin band at 1,600.0 cm^{-1}). (F) Fluorescent, high background component between and within tracheids and vessels. (G) Component including lipids (yellow spectrum). (H) Combined image showing the dominance of fibers (blue), which are differentiated from S_1 of fibers, tracheids, and vessels (cyan) by the higher cellulose microfibril angle. The highest lignin content (red) is found between the cells. Fluorescing components (orange) and lipids (yellow) are mainly in the lumen and along the ray.

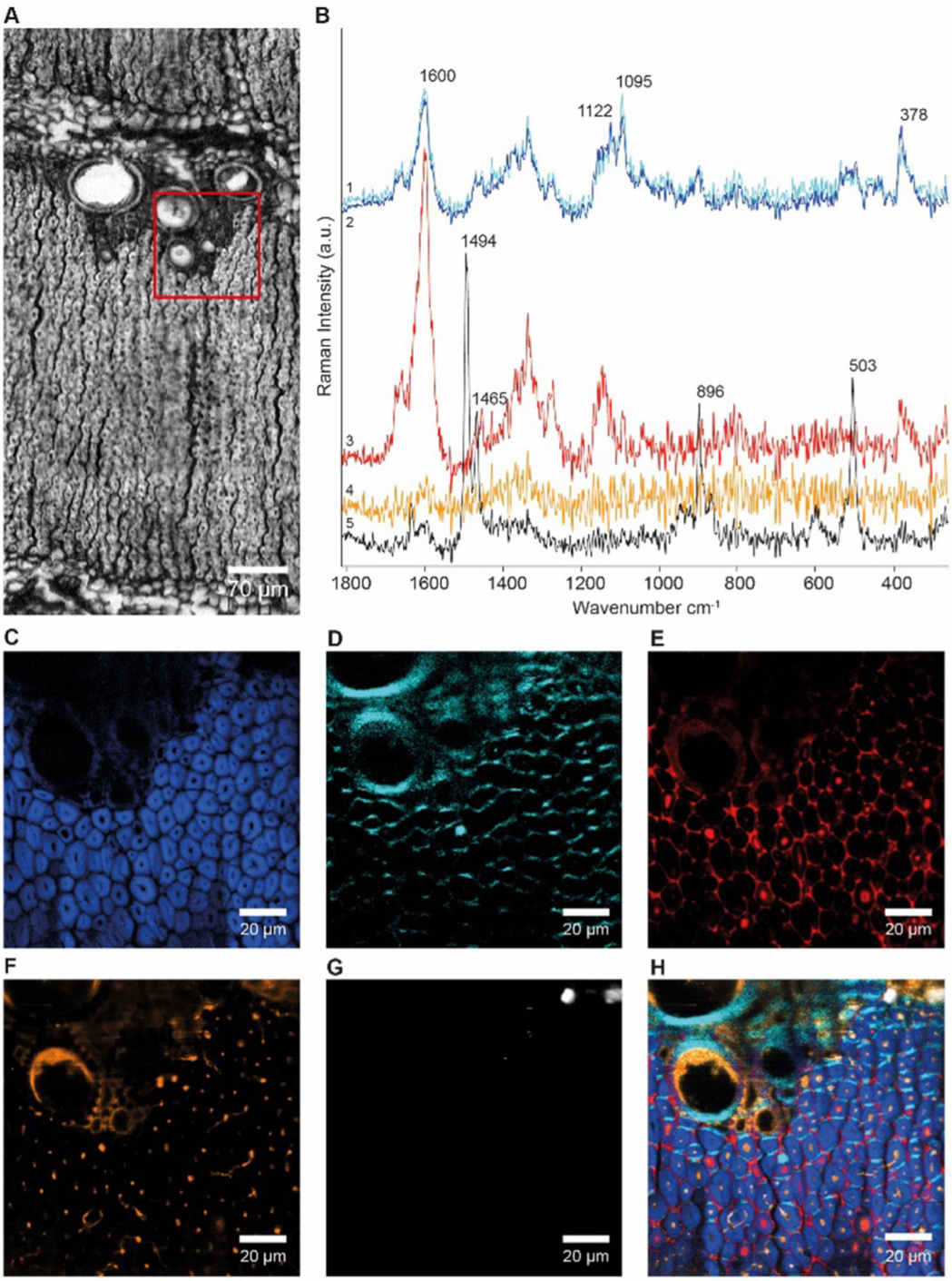

Figure 3: Raman images and spectra of *Haloxylon* heartwood derived by true component analysis. (A) Light microscopic stitching image showing the scanned region of interest, including fibers as well as tracheids and vessels. (B) Five different component average spectra corresponding to (C–G). (C) Cellulose-rich fibers building the main tissue with their S_2-layers (blue spectrum). (D) S_1-layers of the fibers, tracheids, and vessels (cyan spectrum). (E) High-lignin regions in middle lamella and cell zwickels (red spectrum, high-intensity lignin band at 1,600 cm^{-1}). (F) Fluorescent, high-background component. (G) Component with sharp bands (black spectrum) identified as calcium oxalate monohydrate. (H) Combined image showing the increase of the fluorescing extractive component (orange) in the heartwood compared to the sapwood (*cf.* Figure 2F).

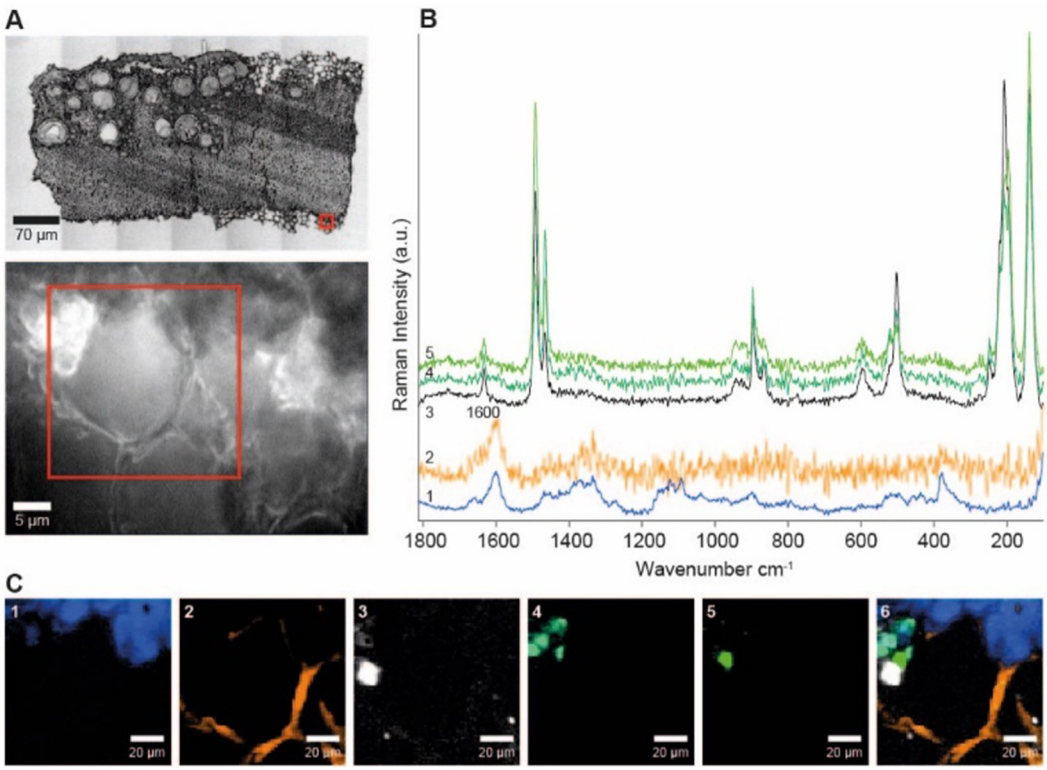

Figure 4: Raman images and spectra of *Haloxylon* heartwood derived by true component analysis. (A) Light microscopic stitching image showing the scanned region of interest including the thin cells at the borders to the thick-walled fibers. (B) Five different component average spectra corresponding to pictures 1–5 in (C): 1: thick-walled fibers; 2: thin-walled cells; 3–5: calcium oxalate monohydrate crystals; 6: combined image showing the different crystal planes separated and the abrupt border between thick-walled fibers and parenchyma cells.

a high fluorescence background (more noise) and an aromatic band at 1,600 cm^{-1} it was assumed that also these thin cell walls are impregnated with lignin and/or extractives. One of the border cells is filled with a big crystal, while smaller ones are observed in the other cells.

For the crystals, three different Raman spectra were obtained with changing heights of the different bands (Figure 4B, spectrum 3–5), according to the different crystal plane orientation with respect to the laser direction. Calcium oxalate crystals are known to protect the plant from a variety of environmental stresses and play a role in tissue calcium regulation, defense against herbivores, and metal detoxification (Nakata 2003). However, under a particularly dry environment, calcium oxalate crystals can also serve as an internal CO_2 source, thus providing adaptive advantages under drought conditions when stomata are closed (Tooulakou et al. 2016). Calcium oxalate crystals are more and more seen as a dynamic source that releases CO_2 and water molecules upon decomposition, which appears to be essential under drought conditions and explains the prominent occurrence in plants thriving in arid climates (Franceschi and Nakata 2005; Karabourniotis et al. 2020) . Besides the physiological and defensive function, $Ca(COO)_2{*}H_2O$ crystals in sclerenchyma cells were also reported as a successful strategy to improve the rigidity in case of pecan nutshells (Arzate-Vázquez et al. 2022).

3.2 Mechanical properties

The density (ρ), modulus of elasticity (ε), and compression strength (σ_t) of *H. ammodendron* untreated natural wood (Figure 5A) were examined in comparison to European beech (*Fagus sylvatica*), a commercially important wood native to Eurasia and North America (Figure 5B).

The density (ρ) of *H. ammodendron* clear wood was measured to range between 1,108.3 and 1,144.2 kg/m^3, which is comparable to the literature value of *Guaiacum officinale* or *Lignum vitae*, one of the heaviest woods in trade, with an average density of ca. 1,120.0 kg/m^3 (Yin et al. 2016). While *H. ammodendron* wood is among the hardest woods, its modulus of elasticity (ε) was significantly lower (between 0.96 GPa and 1.7 GPa with a means of 1.2 GPa). This is explained by micro-irregularities in the wood structure, such as curved grain structure, and density which are all part of the environmental adaptation strategies of *H. ammodendron* (Table 1).

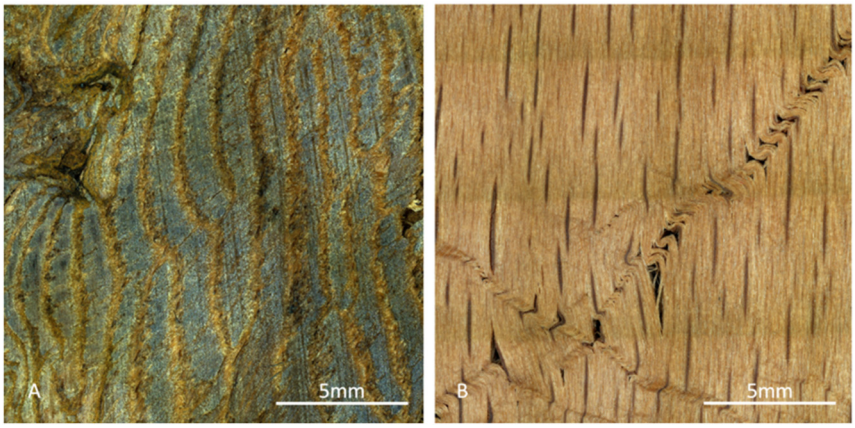

Figure 5: Compared microscopic images of (A) *Haloxylon ammodendron* and (B) *Fagus sylvatica* untreated natural wood cross-sections after mechanical testing.

Table 1: Overview of mechanical properties of *Haloxylon ammodendron* compared to *Fagus sylvatica* as a reference.

	F. sylvatica			*H. ammodendron*		
Statistical indicator	**ε (GPa)**	**σ_t (MPa)**	**ρ (kg/m^3)**	**ε (GPa)**	**σ_t (MPa)**	**ρ (kg/m^3)**
n	3	3	3	3	3	3
Mean	2.2	71.2	682.4	1.2	25.1	1,120.9
Min.	1.9	67.7	671.6	0.9	20.2	1,108.3
Max.	2.4	73.0	690.0	1.6	27.7	1,144.2

Ecological trends reflected in the wood anatomy of various Chenopodiaceae from extreme habitats in Asia, Australia, North America, and the Mediterranean are seen also in *H. ammodendron* in the form of short (50.0–90.0 µm) vessel elements, narrow vessels, in combination with thick to very thick-walled fibers with an average length 286.0 µm (Heklau et al. 2012; Nooshin 2012) which defines its lower mechanical properties.

This includes smaller cell cavities, increased mass per volume, and greater mechanical resistance (Zhou and Gong 2017). The weak compression strength (σ_t), parallel to grain averaging 25.1 MPa, also characterized by the wood density, structural inhomogeneity reflects the brittleness of natural *H. ammodendron* wood (Figure 6). The ultrastructural inhomogeneity in "clear" wood samples, along with the presence of crystals in parenchyma cells and the higher proportion of short fiber makes *H. ammodendron* wood highly brittle, exhibiting minimal deformation and a poor capacity to withstand compressive stress. We also assume that the low moisture content contributes greatly to the mechanical properties (not shown here) and making the wood less suitable for any applications requiring flexibility.

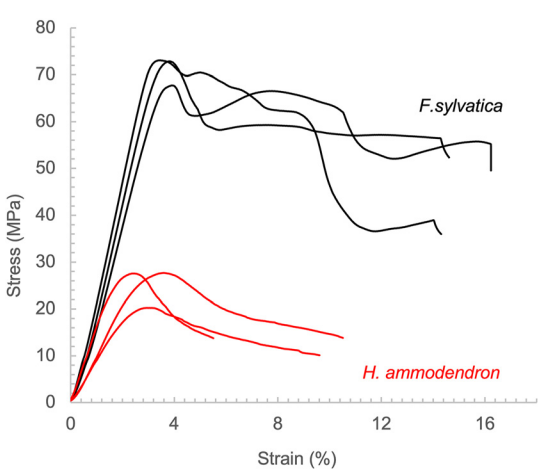

Figure 6: A compressive strength test (parallel to grain) of *Haloxylon ammodendron* and *Fagua sylvatica*.

Literature is scarce regarding the properties of *H. ammodendron* wood. Especially, follow-up research is needed to reveal the variation in properties and deterioration of *H. ammodendron*, caused by the mechanical damages, the attack by parasitic fungi and plants (Naran et al. 1995), and exposure to the extreme Gobi Desert environment.

3.3 Chemical analysis of *H. ammodendron* wood

3.3.1 Lignin content

The bulk amount of lignin was determined by comparing the amount of precipitation after the Klason method (acid-

insoluble lignin), while the acid-soluble lignin was determined by the UV method, apart from extractives and sugar components in *H. ammodendron*. The mass ratios of both dried acid-insoluble (Klason) and soluble lignins in the *H. ammodendron* wood dry sample were calculated as 258.6 mg/g and 17.6 mg/g. The respective percentage of Klason lignin corresponds well within the variable range of lignin in various wood species, including high-density tropical woods (Gérard et al. 2019).

A detailed study of the structure of *H. ammodendron* lignin will be reported in due course.

3.3.2 Carbohydrate profile by methanolysis

A detailed quantitative analysis of cell wall composition (e.g., cellulose, hemicellulose, and lignin content) is important for the future processing of *H. ammodendron* wood.

Determination of monosaccharide profiles used the acidic methanolysis protocol (Sundberg et al. 1996) which involves quantification by GC after suitable derivatization of the released mixture of methyl pyranosides and furanosides (Becker et al. 2013a,b).

The methanolysis gave a total sugar amount of 358.75 µg/mg of dry matter. It should be noted that acidic methanolysis covers all hemicelluloses and amorphous cellulose contributions, but not the crystalline, recalcitrant cellulose parts.

The most abundant sugars identified in the dry matter are xylose, galactose, and arabinose (with relative contents of 224.5, 26.4, and 24.1 µg/mg, respectively), followed by amounts of rhamnose (9.8 µg/mg), glucose (7.9 µg/mg), mannose (1.8 µg/mg), and fucose (1.1 µg/mg). Minor amounts of acidic sugars, such as glucuronic- (2.4 µg/mg), galacturonic- (20.8 µg/mg), and 4-*O*-methyl glucuronic (39.8 µg/mg) acids, all critical with regard to pulp and paper chemistry (Sundberg et al. 1998), were also detected with a sum of 63.0 µg/mg. Especially the relatively high yield of 4-*O*-methylglucuronic acid, an important constituent in hardwood, together with arabinose, and galactose indicates the presence of glucuronoxylan in *H. ammodendron*.

3.3.3 Extractives

The cumulative amount of non-structural wood extractives in *H. ammodendron* was calculated as 5.9 % of its dry weight, after sequential fractionation with organic solvents of different polarity. Wood extractives function as defensive compounds vital to the performance of wood species (Kirker et al. 2013). As individual compounds in extractives are primarily responsible for the resistance of wood against their biological enemies, the identification of those compounds and the general composition of *H. ammodendron* extractives are of further interest and are currently being studied.

4 Conclusions

H. ammodendron is a prominent but unknown as renewable resource wood species. This study examines the ultrastructure, mechanical properties, and general chemical composition of the *H. ammodendron* wood growing in the Mongolian Gobi.

in situ Raman imaging of *H. ammodendron* wood tissue visualized the impregnation with extractives throughout the tissue and accumulation of calcium oxalate monohydrate at the tissue border. Both constituents can directly contribute to structure-chemical defense mechanisms. The results presented here will be helpful in future studies for a better understanding of the relation of structure and non-structural extractives in response to extreme environmental conditions, for the case of *H. ammodendron* wood and generally in plants.

Its anatomy has prominent elements of ecological trends from the extreme environment of the Gobi Desert to moist tropical forest, very thick-walled, high density fiber cells, tracheids, and the vessels guarded by the high amount of lignins, which allow secure transport. Considering the importance of this species to combat desertification and its ecological and economic value it holds a promise as a precursor for the development of sorbent materials. Unfortunately, the mechanical properties limit its use in various applications which require flexibility. This research delivers an important contribution to the sustainable development of *H. ammodendron* desert communities.

Acknowledgments: The authors thank Dr. Ivan Sumerskii, Dr. Sonja Schiehser for technical support, as well as Dr. Oliver Musl, and Dr. Jan Janesch for helpful discussions. Open access funding was provided by the University of Natural Resources and Life Sciences Vienna (BOKU). The support of the Austrian Biorefinery Center Tulln (ABCT_II) is gratefully acknowledged.

Research ethics: We state that the study was conducted in accordance with the Declaration of Helsinki (as revised in 2013).

Informed consent: Informed consent was obtained from all individuals included in this study.

Author contributions: The authors have accepted responsibility for the entire content of this manuscript and approved its submission.

Use of Large Language Models, AI and Machine Learning Tools: None declared.

Conflict of interest: The authors state no conflict of interest.
Research funding: This work was supported by funding from the Austrian Agency for Education and Internationalization, Federal Ministry of Education, Science and Research of Austria, Project KoEF 10/2020 awarded to DG.
Data availability: The raw data can be obtained on request from the corresponding author.

References

Arzate-Vázquez, I., Méndez-Méndez, J.V., Nicolás-Bermúdez, J., Chanona-Pérez, J.J., Domínguez-Fernández, R.N., and Vélez-Rivera, N. (2022). Effect of calcium oxalate crystals on the micromechanical properties of sclerenchyma tissue from the pecan nutshell (*Carya illinoinensis*). *Plant Physiol. Biochem.* 170: 249–254.

Azhar, M.F., Aziz, A., Haider, M.S., Nawaz, M.F., and Zulfiqar, M.A. (2015). Exploring the ethnobotany of *Haloxylon recurvum* (Khar) and *Haloxylon salicornicum* (Lana) in cholistan desert, Pakistan. *Pak. J. Agricultural Sci.* 52: 1085–1090, https://api.semanticscholar.org/CorpusID:89771144 (Accessed 01 December 2024).

Becker, M., Zweckmair, T., Forneck, A., Rosenau, T., Potthast, A., and Liebner, F. (2013a). Evaluation of different derivatisation approaches for GC/MS analysis of carbohydrates in complex matrices of biological and synthetic origin. *J. Chromatogr. A* 1281: 115–126.

Becker, M., Liebner, F., Rosenau, T., and Potthast, A. (2013b). Ethoximation-silylation approach for mono- and disaccharide analysis and characterization of their identification parameters by GC/MS. *Talanta* 115: 642–651.

Bock, P. and Gierlinger, N. (2019). Infrared and Raman spectra of lignin substructures: coniferyl alcohol, abietin, and coniferyl aldehyde. *J. Raman Spectrosc.* 50: 778–792.

Bock, P., Nousiainen, P., Elder, T., Blaukopf, M., Amer, H., Zirbs, R., Potthast, A., and Gierlinger, N. (2019). Infrared and Raman spectra of lignin substructures: dibenzodioxocin. *J. Raman Spectrosc.* 51: 422–431.

Deutsches Institut für Normung (1976). *Prüfung von Holz; Bestimmung der Rohdichte (DIN 52182:1976-09)*. DIN Media GmbH, Berlin.

Dorjsuren, C. (2021). *Forest Inventory of Mongolia, Technical Report*. The Centre for Forest Research and Development, Ulaanbaatar.

Fan, L., Wang, G., Hu, W., Pantha, P., Tran, K.-N., Zhang, H., An, L., Dassanayake, M., and Qui, Q.-S. (2018). Transcriptomic view of survival during early seedling growth of the extremophyte *Haloxylon ammodendron*. *Plant Physiol. Biochem.* 132: 475–489.

Franceschi, V. and Nakata, P.A. (2005). Calcium oxalate in plants: formation and function. *Annu. Rev. Plant Biol.* 56: 41–71.

Gérard, J., Paradis, S., and Thibaut, B. (2019). Survey on the chemical composition of several tropical wood species. *Bois. Forêts des Tropiques* 342: 79–91.

Gierlinger, N. (2017). New insights into plant cell walls by vibrational microspectroscopy. *Appl. Spectrosc. Rev.* 53: 517–551.

Gierlinger, N., Luss, S., König, C., Konnerth, J., Eder, M., and Fratzl, P. (2010). Cellulose microfibril orientation of *Picea abies* and its variability at the micron-level determined by Raman imaging. *J. Exp. Bot.* 61: 587–595.

Heklau, H., Gasson, P., Schweingruber, F., and Baas, P. (2012). Wood anatomy of Chenopodiaceae (Amaranthaseae s.l.). *IAWA J.* 33: 205–232.

Hessl, A.E., Anchukaitis, K.J., Jelsema, C., Cook, B., Byambasuren, O., Leland, C., Nachin, B., Pederson, N., Tian, H., and Hayles, L.A. (2018). Past and future drought in Mongolia. *Sci. Adv.* 14: e1701832.

International Organization for Standardization (1976). *Standard atmospheres for conditioning and/or testing; Specifications (ISO 554: 1976)*. International Organization for Standardization, Geneva, Switzerland.

Karabourniotis, G., Horner, H.T., Bresta, P., Nikolopoulos, D., and Liakopoulos, G. (2020). New insights into the functions of carbon–calcium inclusions in plants. *New Phytol.* 228: 845–854.

Kirker, G.T., Blodgett, A.B., Arango, R.A., Lebow, P.K., and Clausen, C.A. (2013). The role of extractives in naturally durable wood species. *Int. Biodeterior. Biodegrad.* 82: 53–58.

Lee, M.-H., Jeon, H.S., Kim, S.H., Chung, J.H., Roppolo, D., Lee, H.-J., Cho, J.H., Tobimatsu, Y., Ralph, J., and Park, O.K. (2019). Lignin-based barrier restricts pathogens to the infection site and confers resistance in plants. *EMBO J.* 38: e101948.

Li, C., Li, Y., and Ma, J. (2011). Spatial heterogeneity of soil chemical properties at fine scales induced by *Haloxylon ammodendron* (Chenopodiaceae) plants in a sandy desert. *Ecol. Res.* 26: 385–394.

Li, J., Wada, H., and Matsuzaki, H. (2015). Radial growth rate through successive cambia in *Haloxylon ammodendron* (Chenopodiaceae) from the Gurbantünggüt Desert, Northwestern China, determined by a series of radiocarbon dating. *Geochem. J.* 49: 39–51.

Liancourt, P., Spence, L.A., Lkhagva, A., Sharkhuu, A., Bodgov, B., Helliker, B.R., Petraitis, P.S., and Casper, B.B. (2013). Plant response to climate change varies with topography, interactions with neighbors, and ecotype. *Ecology* 94: 444–453.

Lin, S.Y., and Dence, C.W. (Eds.) (1992). *Methods in lignin chemistry*. Springer, Berlin-Heidelberg.

Liu, S.-W., Jadambaa, N., Nikandrova, A.A., Osterman, I.A., and Sun, C.-H. (2022). Exploring the diversity and antibacterial potentiality of cultivable actinobacteria from the soil of the saxaul forest in Southern Gobi Desert in Mongolia. *Microorganisms* 10: 989.

Mateu, B.P., Bock, P., and Gierlinger, N. (2020) Raman imaging of plant cell walls. In: Popper, Z. (Ed.). *The plant cell wall. Methods in Molecular Biology*. Humana, New York, pp. 251–295.

Menden, B., Kohlhoff, M., and Moerschbacher, B.M. (2007). Wheat cells accumulate a syringyl-rich lignin during the hypersensitive resistance response. *Phytochemistry* 68: 513–520.

Morel, O. and Gierlinger, N. (2023). Chemical tissue heterogeneity of young *Arabidopsis* stems revealed by Raman imaging combined with multivariate data analysis. *Microchem. J.* 191: 108900.

Moura, J.C.M.S., Bonine, C.A.V., Viana, J.D.O.F., Dornelas, M.C., and Mazzafera, P. (2010). Abiotic and biotic stresses and changes in the lignin content and composition in plants. *J. Integr. Plant Biol.* 52: 360–376.

Nakata, P.A. (2003). Advances in our understanding of calcium oxalate crystal formation and function in plants. *Plant Sci.* 164: 901–909.

Naran, R., Ebringerova, A., and Alfödli, J. (1995). The cell wall material of the wood parasite Cistanche deserticola Y. C. Ma. *Holzforschung* 49: 293–299.

Neilson, E.H., Goodger, J.Q.D., Woodrow, I.E., and Lindberg Møller, B. (2013). Plant chemical defense: at what cost? *Trends Plant Sci.* 18: 250–258.

N'Guessan, J.L.L., Niamké, B.F., Yao, N.J.C., and Amusant, N. (2023). Wood extractives: main families, functional properties, fields of application and interest of wood waste. *For. Prod. J.* 73: 194–208.

Nooshin, T. (2012). Wood features of saxaul (*Haloxylon* spp.) from Central Iran. *World Appl. Sci. J.* 20: 1114–1122, https://www.idosi.org/wasj/wasj20(8)12/8.pdf (Accessed 01 December 2024).

Robert, E.M.R., Schmitz, N., Boeren, I., Driessens, T., Herremans, K., De Mey, J., Van de Casteele, E., Beeckman, H., and Koedam, N. (2011).

Successive Cambia: a developmental oddity or an adaptive structure? *PLOS One* 6: e16558.

Schneider, H.M. (2022). Characterization, costs, cues and future perspectives of phenotypic plasticity. *Ann. Bot.* 130: 131–148.

Sundberg, A., Sundberg, K., Lillandr, C., and Holmbom, B. (1996). Determination of hemicelluloses and pectins in wood and pulp fibres by acid methanolysis and gas chromatography. *Nord. Pulp. Pap. Res. J.* 4: 216–226.

Sundberg, K., Sundberg, A.C., Thornton, J.W., and Holmbom, B.R. (1998). Pectic acids in the production of wood-containing paper. *Tappy J.* 81: 131–136, https://api.semanticscholar.org/CorpusID:101777724 (Accessed 10 Oct 2024).

Tooulakou, G., Giannopoulos, A., Nikolopoulos, D., Bresta, P., Dotsika, E., Orkoula, M.G., Kontoyannis, C.G., Fasseas, C., Liakopoulos, G., Klapa, M.I., et al. (2016). Alarm photosynthesis: calcium oxalate crystals as an Internal CO_2 source in plants. *Plant Physiol.* 171: 2577–2585.

Tronchet, M., Balagué, C., Kroj, T., Jouanin, l., and Roby, D. (2010). Cinnamyl alcohol dehydrogenases-C and D, key enzymes in lignin biosynthesis, play an essential role in disease resistance in Arabidopsis. *Mol. Plant Pathol.* 11: 83–92.

Yin, W., Shan, L., Lu, H., Zheng, Y., Han, Z., and Tian, Y. (2016). Impact resistance of oil-immersed lignum vitae. *Sci. Rep.* 6: 30090.

Zhou, C.B. and Gong, W. (2017). Effect of provenance and climate on xylem anatomy of *Haloxylon ammodendron* (C. A. Mey) Bunge in the Gurbantunggut desert, China. *Appl. Ecol. Environ. Res.* 15: 1309–1321.